

Exploring Mechanisms of Hydration and Carbonation of MgO and Mg(OH)₂ in Reactive Magnesium Oxide-based Cements

Mina Ghane Gardeh,^a Andrey A. Kistanov,^{*,b} Hoang Nguyen,^a Hegoi Manzano,^c Wei Cao,^b and Paivo Kinnunen^a

^aFibre and Particle Engineering Research Unit, University of Oulu, Pentti Kaiteran katu 1, 90014 Oulu, Finland.

^bNano and Molecular Systems Research Unit, University of Oulu, Pentti Kaiteran katu 1, 90014 Oulu, Finland.

^cDepartment of Condensed Matter Physics, University of the Basque Country (UPV/EHU), Barrio Sarriena, s/n, 48940 Leioa, Spain.

***Corresponding author:** andrey.kistanov@oulu.fi

Abstract

Reactive magnesium oxide (MgO)-based cement (RMC) can play a key role in carbon capture processes. However, knowledge on the driving forces that control the degree of carbonation and hydration and rate of reactions in this system remains limited. In this work, density functional theory-based simulations are used to investigate the physical nature of the reactions taking place during the fabrication of RMCs under ambient conditions. Parametric indicators such as adsorption energies, charge transfer, electron localization function, adsorption/dissociation energy barriers and the mechanisms of interaction of H₂O and CO₂ molecules with MgO and brucite (Mg(OH)₂) clusters are considered. The following hydration and carbonation interactions relevant to RMCs are evaluated: *i*) carbonation of MgO, *ii*) hydration of MgO, carbonation of hydrated MgO, *iii*) carbonation of Mg(OH)₂, *iv*) hydration of Mg(OH)₂ and *v*) hydration of carbonated Mg(OH)₂. A comparison of the energy barriers and reaction pathways of these mechanisms shows that the carbonation of MgO is hindered by presence of H₂O molecules, while the carbonation of Mg(OH)₂ is hindered by the formation of initial carbonate and hydrate layers as well as presence of excess H₂O molecules. To compare these findings to bulk mineral surfaces, the interactions of the CO₂ and H₂O molecules with the MgO(001) and Mg(OH)₂(001) surfaces are studied. Therefore, this work presents deep insights into the physical nature of the reactions and the mechanisms involved in hydrated magnesium carbonates production that can be beneficial for its development.

Keywords: Magnesium oxide, brucite, DFT, clusters, carbon capture

Introduction

Increasing carbon dioxide (CO₂) emissions are currently one of the most serious environmental challenges.¹ Cement manufacturing, and specifically the manufacture of ordinary Portland cement (OPC), is the source of ~5%–7% of global greenhouse gas emissions.² Limestone (CaCO₃), the conventional feedstock for OPC manufacturing, is excavated, crushed and sintered with other materials in a cement kiln at temperatures reaching ~1450°C to produce clinker. During the calcination of CaCO₃, CO₂ is directly emitted (i.e. CaCO₃ → CaO + CO₂), causing ~50%–60% of the total emissions from OPC production.³ From the standpoint of sustainable development, the cement industry is seeking alternatives to reduce CO₂ emissions while maintaining the same performance.⁴

Among the proposed alternative binders, Mg-based cements have attracted attention for their promise as partial replacements for OPC.⁵ When magnesium oxide (MgO) is derived from Mg silicates (e.g. olivine and serpentine), less environmental and economic impact is generated.⁶ The net CO₂ emissions from the carbonation of these binders may be ~73% lower than OPC,⁷ and, therefore, may potentially lead to the formation of carbon-negative cements. Moreover, the lower production temperature of reactive MgO-based cement (RMC) compared to that of OPC (i.e. 700–1000°C vs. 1450°C), and its potential to gain strength through its reaction with CO₂, has attracted special attention.⁷

Considering the need for the rapid development of carbon capture and utilisation technology,⁸ the main advantage of RMCs produced from Mg-Si minerals in concrete formulations is their ability to absorb and permanently store CO₂ in the form of stable carbonates during the carbonation process, when MgO is sourced from low-CO₂ feedstocks.⁹ In such processes, MgO reacts with water (H₂O) to form brucite (Mg(OH)₂), which generally has a weak and porous structure.^{5,10} However, hydrated MgO has a strong ability to absorb CO₂ and produce carbonated products at a strength useful for construction purposes.¹¹ In other words, the dissolution of MgO through hydration results in the formation of Mg(OH)₂, which is then carbonated according to the following reaction and produces a range of hydrated magnesium carbonates (HMCs): Mg(OH)₂ + CO₂ + 2H₂O → MgCO₃·3H₂O. Nesquehonite (MgCO₃·3H₂O) is the most commonly obtained HMC, yet other phases such as hydromagnesite (4MgCO₃·Mg(OH)₂·4H₂O), dypingite (4MgCO₃·Mg(OH)₂·5H₂O) and artinite (MgCO₃·Mg(OH)₂·3H₂O) can also be present.^{12,13}

Recent experimental studies have examined the formation of HMCs through the hydration and carbonation of RMC. In particular, improvement of the hydration and mechanical performance of carbonated MgO-based systems has been observed with the introduction of various hydration agents at different concentrations.¹⁴ In this way, the simultaneous use of magnesium acetate at 0.05 M and carbonate seeds (up to 1% of cement content) improved mechanical performance of carbonated RMC concrete mixes.¹⁵ However, investigation of the physical nature of mechanisms involved in the reactions of HMC production is still immature. One of the reasons for this is the limitation of available experimental methods for the determination of such processes occurring at the nanoscale in bulk materials.

Theoretical approaches with predictive capabilities, such as those based on the density functional theory (DFT), show a high capability for determining the most stable atomic structures and exploring the physical and chemical properties of these finite systems.^{16,17,18,19} Computational approaches have been successfully utilised to investigate in depth the mechanisms related to the formation of HMCs. For instance, the structure, formation energy and electronic properties of four commonly exposed surfaces of nesquehonite crystal have been studied using DFT-based calculations.¹⁶ In another computational work the activity and selectivity of MgO surfaces for CO₂ conversion have been studied.²⁰ In particular, the adsorption and dissociation of CO₂, as well as its

subsequent hydrogenation to HOCO and HCOO, on various MgO surfaces, have been investigated. It has been shown that the direct dissociation of CO₂ on MgO is thermodynamically unfavourable because of high reaction energy, while hydrogenation of CO₂ to HCOO by hydride H is more feasible on MgO. DFT simulations have also been utilised to compare the adsorption and activation reaction mechanisms of CO₂ and H₂ molecules on hydrogen-assisted MgO(110), pure Ni(111) and Ni/MgO interfaces.²¹ Computational methods have also been applied for a deeper exploration of the effects of various promoters and dopants upon CO₂ adsorption on the MgO–CaO(100) surface.²² Theoretically supported experimental infrared-based studies have been performed to identify the structure of the CO₂ species adsorbed on the various MgO surface.²³ It has been shown that the active site towards CO₂, which is a Lewis acid, differs from that for the deprotonating adsorption of Brønsted acids. Another experimentally supported computational study provided a comprehensive study on the CO₂ adsorption on the MgO and Mg(OH)₂ surfaces.²⁴ It has been found that chemisorption of CO₂ on the MgO surface is facilitated by the presence of H₂O.

Since the reaction degrees of MgO and Mg(OH)₂ are relatively low (ca. 50%), they reduce the effectiveness of CO₂ utilization to form a cementitious binder.²⁵ Furthermore, because the transformation of HMCs shows mixed diffusion and reaction-limited control, and it proceeds through the production of metastable intermediates, the specifics of nesquehonite conversion to other HMCs remains unclear. The conversion of these metastable intermediates also raises concerns about the durability of cement.²⁶ Therefore, insights into the potential reactions in the MgO/H₂O/CO₂ system, and an understanding of the nature of kinetic hindrance in MgO and Mg(OH)₂ carbonation and hydration at the atomic level, are of immediate interest.

In this work, the physical nature of the mechanisms for HMC production on MgO and Mg(OH)₂ nanoclusters is considered using DFT calculations. Clusters are collections of atoms that act as a link between gases and bulk phase materials (liquids and solids). They are considerably large to be considered as molecules while considerably small to be classified as liquids or solids, and almost all of the atoms in a cluster are on or near its surface, making them a good choice for considering surface reactions.²⁷ In addition, robust reactions at oxide surfaces, such as the exchange rates of H₂O molecules on the surface can be reliably predicted using molecular-simulation methods.²⁸

Here, the interaction of these nanoclusters of potentially promising RMC raw materials with ambient molecules (H₂O and CO₂) is considered. The mechanism of the following reactions is investigated: carbonation of MgO, hydration of MgO, carbonation of hydrated MgO, carbonation of Mg(OH)₂, hydration of Mg(OH)₂ and hydration of carbonated Mg(OH)₂. Notably, even though through-solution dissolution–precipitation reactions are often the dominating reactions in HMC synthesis, surface carbonation can become important to the overall carbonation kinetics by hindering further reactions, including dissolution. Understanding the mechanisms of these reactions is accomplished by calculating adsorption energy, charge transfer, electron localization function and adsorption/dissociation energy barriers of H₂O and CO₂ upon reactions with the MgO and Mg(OH)₂ clusters. To gain further insights into the difference between MgO and Mg(OH)₂ clusters and bulks, the interactions between the surfaces of bulk MgO and Mg(OH)₂ with H₂O and CO₂ molecules are also investigated. The results also shed light on the underlying reason for the hindrance of carbonation of MgO and Mg(OH)₂ that has been previously observed experimentally. Therefore, the results of this work reveal the mechanisms that take place during HMC production that can further facilitate the development of their production.

Methods

The calculations were carried out based on DFT using the Vienna ab-initio simulation package²⁹ where the electron–ion interactions were simulated via the projector augmented wave method.³⁰ The

generalized gradient approximation with the of Perdew–Burke–Ernzerhof exchange-correlation function was employed.³¹ The most energetically favourable MgO cluster has a cage-like configuration with T_h symmetry that included six Mg_2O_2 rings and eight Mg_3O_3 to form a shortened octahedron with equivalent Mg and O vertices.³² The system considered consisted of a MgO cluster placed in a cubic supercell with dimensions of $20 \times 20 \times 20 \text{ \AA}$. A $3 \times 3 \times 3$ k-point sampling was employed for structure optimization calculations, while a $1 \times 1 \times 1$ k-point was used for electronic structure calculations. $Mg(OH)_2$ cluster consisting of 9 units of $Mg(OH)_2$ ³³ was placed in a cubic cell with dimensions of $30 \times 30 \times 30 \text{ \AA}$. A $1 \times 1 \times 1 \text{ \AA}$ k-point sampling was applied for all optimisation and electronic structure calculations. The considered MgO and the $Mg(OH)_2$ slabs with the (001) cleaved-plane surface were selected based on the previous work.³⁴ A $2 \times 2 \times 1 \text{ \AA}$ and $1 \times 1 \times 1 \text{ \AA}$ k-point sampling was used for MgO and $Mg(OH)_2$ slabs, respectively.

All systems considered were totally optimized to reach atomic forces and total energies less than 0.05 eV \AA^{-1} and 10^{-4} eV , respectively. A kinetic energy cut-off of 450 eV was set for all calculations. The van der Waals–corrected functional Becke88 optimisation (optB88)³⁵ was adopted for the consideration of non-covalent chemical interactions between molecules and clusters. The adsorption energy of the molecule is given by the following equation³⁶:

$$E_{ads} = E_{molecule/cluster} - (E_{molecule} + E_{cluster}), \quad (1)$$

where $E_{molecule/cluster}$ is the total energy of the cluster with the adsorbed molecule, $E_{molecule}$ is the total energy of the isolated molecule and $E_{cluster}$ is the total energy of the bare cluster. Under this definition, the negative adsorption energy indicates an exothermic and favourable process. The electrons gained or lost are defined as the difference of valence electrons of an atom in the adsorbed system from the atom in a free molecule or a substrate, according to the equation $\Delta q = q_{after \text{ adsorption}} - q_{before \text{ adsorption}}$. The negative and positive values indicate electrons gained and lost, respectively.

The charge transfer between the molecule and the cluster is given by the charge density difference (CDD) $\Delta\rho(r)$:

$$\Delta\rho(r) = \rho_{cluster+molecule}(r) - \rho_{cluster}(r) - \rho_{mol}(r), \quad (2)$$

where $\rho_{cluster+molecule}(r)$, $\rho_{cluster}$ and $\rho_{mol}(r)$ are the charge densities of the cluster with the adsorbed molecule, the bare cluster and the isolated molecule, respectively. The Bader analysis was used to calculate the charge transfer between the molecules and the clusters³⁷.

The Arrhenius equation is given by the following formula:

$$k = Ae^{-E_b/RT}, \quad (3)$$

where k is the rate constant, A is the pre-exponential factor, E_b is the activation energy or the energy barrier for a reaction, R is the universal gas constant, and T is the absolute temperature.³⁸

The electron localisation function (ELF) was calculated to obtain the distribution of electrons in the considered structures. The degree of charge localisation in real space is depicted by the value of the ELF (between 0 and 1), where 0 represents a free electronic state and 1 represents a perfect localisation. An isosurface value of 0.65 was adopted in this work.³⁹

The climbing image–nudged elastic band (CI-NEB) method⁴⁰ was used to obtain the reaction pathway of the molecule on the cluster. The AIMD simulations were carried out at room temperature

of 300 K. The simulation lasted for ~5 ps with a time step of 1 fs, and the temperature was controlled by a Nose–Hoover thermostat.⁴¹

Results and Discussion

MgO interaction with CO₂ and H₂O. The interaction of the MgO cluster with the CO₂ molecule is considered to simulate the formation of MgO–CO₂ (MgCO₃) as the main precursor to HMCs. For this, various absorption configurations of the CO₂ molecule on the MgO cluster are considered (more details see Figure S1 in Supporting Information). Figure 1a shows the lowest-energy configuration structure of the CO₂ molecule adsorbed on the MgO cluster, combined with the CDD plot. In the most stable configuration, the O atom of the CO₂ molecule is bonded to the Mg atom of the MgO cluster. The length of the created Mg–O bond is 2.207 Å. The length of the C–O bond of the CO₂ molecule is elongated from 1.174 Å (bare CO₂) to 1.188 Å (CO₂ after adsorption on MgO). It is also found that the ∠(O–C–O) angle of CO₂ adsorbed on the MgO cluster decreases to 171.94° compared to 179.95° for the bare CO₂. Table S1 (see Supporting Information) combines the results for the adsorption energy E_{ads} and charge transfer Δq between the CO₂ molecule and the MgO cluster. It is shown that E_{ads} of the CO₂ molecule on the MgO cluster is -0.42 eV. According to the CDD plot (see Figure 1a), the CO₂ molecule acts as an acceptor to the MgO cluster with the charge transfer from the surface to the molecule of 0.092 e (see Table S1 in Supporting Information), which can be attributed to the basicity of the MgO cluster, as it can donate a pair of nonbonding electrons following the Lewis base role.²¹ The observed elongation of the C–O bond and the enhanced charge transfer between the cluster and molecule suggest a strong interaction between them. The high electronegativity of O atoms of the molecule can be the driving force for the observed charge transfer compared to that of Mg atoms of the cluster. However, the ELF analysis (see Figure 1b) shows that electron density is mainly located at the Mg–O bond, which indicates electron depletion from the surface of the cluster to the CO₂ molecule, and at the O atoms of the CO₂ molecule, indicating that strong covalent bonding remains only within the molecule.

To deeper understand the interaction of the CO₂ molecule with the MgO cluster, density of states (DOS) and local density of states (LDOS) analyses of CO₂-adsorbed MgO are performed (see Figure 1c). The bare MgO cluster has higher HOMO and HOMO-1 states than the CO₂ molecule, which indicates its tendency to oxidize the molecule, whereas the CO₂ molecule possess LUMO and LUMO+1 states, which verifies its ability to gain electrons. Moreover, strong overlapping of LUMO and LUMO+1 states is observed upon the interaction between the molecule and the cluster, suggesting a strong interaction between them. In addition, AIMD simulations are conducted to study the interaction of the CO₂ molecule with the MgO cluster at room temperature. The AIMD calculations (see Movie 1 in Supporting Information) confirm the possibility of the chemisorption of CO₂ on the MgO cluster at room temperature and suggests a low energy barrier E_b for the reaction, as it is proposed from the E_a and charge transfer calculations. Therefore, the chemisorption process of CO₂ on MgO is further considered.

The chemisorbed configuration of CO₂ is chosen based on the AIMD-obtained configuration (see Figure S2 in Supporting Information). In that case, the length of the Mg–O bond formed between the cluster and the molecule is 2.080 Å, which is shorter than that in the physisorbed state (2.207 Å). The length of the newly formed Mg–O bond in the chemisorbed configuration is 2.092 Å. The C–O bond lengths of the CO₂ molecule are 1.269 Å and 1.266 Å, which are significantly longer than those of the CO₂ in its physisorbed state (1.188 Å). This indicates that C–O bonds of CO₂ are highly elongated upon its interaction with Mg atoms. The ∠(O–C–O) angle of 179.95° of bare CO₂ decreases to 129.69° for CO₂ adsorbed on the MgO cluster. The CDD plot (see Figure 1d) and the Bader charge transfer analysis (see Table S1 in Supporting Information), predict that CO₂ is an acceptor to MgO as

it accumulates 0.117 e from the MgO cluster. The amount of charge transferred from MgO to chemisorbed CO₂ is higher than that from MgO to physisorbed CO₂ (see Table S1 in Supporting Information). Furthermore, E_{ads} of CO₂ on MgO in its chemisorbed state is -1.05 eV (see Table S1 in Supporting Information), which is more than twice higher than that of CO₂ physisorbed on MgO. From Figure 1e, which shows ELF of CO₂ chemisorbed on MgO, it is seen that electron localization is located on the C–O bond formed between CO₂ and MgO. In addition, strong electron redistribution is observed on O atoms of CO₂ suggesting the formation of covalent bonds between the molecule and the cluster while the C–O covalent bonds of the CO₂ molecule remain stable. That contributes to the depletion of electrons from the surface to the molecule as it is observed in the CCD plot in Figure 1d.

According to the DOS and LDOS plots in Figure 1f, there is a strong hybridization of the HOMO, HOMO-1 and LUMO+1 states of the MgO cluster and the CO₂ molecule, indicating a strong interaction between them and signifying the possibility of chemisorption of the CO₂ molecule on the MgO cluster. The AIMD simulations also suggest that the chemisorption of CO₂ on MgO is favourable (see Movie 1 and Figure S2 in Supporting Information). Thus, the possible reaction mechanism for the transformation process for the CO₂ molecule on the MgO cluster from physisorbed to chemisorbed state is further studied through NEB approach. The energy profile and related atomic configurations for the initial state (IS), transition state (TS), intermediate states (IM) and final state (FS), showing the transition of the CO₂ molecule from the physisorbed state to the chemisorbed state, are depicted in Figure 1g. TS with an energy level of 0.049 eV proposes the low energy barrier E_b for this transition (see Table S2 in Supporting Information). It seems that the O atom of CO₂ has a high tendency to oxidize the Mg atom of the cluster. This oxidation is expedited at IM3 by the approach and further bonding of the C atom of the molecule to the O of the cluster, which leads to a drop of E_b to 0.001 eV. At FS, the second O atom of CO₂ is bonded to the Mg atom of the cluster, and E_b further drops to -0.617 eV which suggests the reaction is exothermic.

To summarize, the elongation of the C–O bond and the decrease of the $\angle(\text{O–C–O})$ angle of the CO₂ molecule upon its chemisorption on the MgO cluster comparing to physisorption lead to an increase of E_a .²⁴ In addition, higher charge transfer from the cluster to the CO₂ molecule during chemisorption stabilizes the adsorption of the CO₂ molecule on the cluster⁴². These results are well agreed with found low E_b of exothermic transition of CO₂ from physisorbed state to chemisorbed state and with experimental observations confirming that the calcination of magnesite (MgCO₃) is an endothermic process.⁵ Therefore, the chemisorption of CO₂ on MgO occurs favourably under the reaction conditions.

The reaction of H₂O with MgO leads to the formation of Mg(OH)₂, a phase that might also undergo carbonation, which results in the HMC formation. Hence, the hydration of the MgO cluster is also investigated. All possible absorption configurations of H₂O on the MgO cluster are considered (see Figure S3 in Supporting Information). According to Table S1 (see Supporting Information), E_{ads} for the most energetically favourable configuration of adsorbed H₂O on the MgO cluster (see Figure 2a) is -0.95 eV. In this configuration, the Mg–O bond between the O atom of the H₂O molecule and the Mg atom of the MgO cluster and the H–O bond between the H atom of the molecule and the O atom of the cluster are formed. The length of the Mg–O and H–O bonds is found to be 2.085 Å and 1.627 Å, respectively. Moreover, the length of the H–O bond of the H₂O molecule before bonding to the cluster is 0.936 Å, and it is elongated to 1.036 Å after adsorption, signifying the tendency of H₂O to bind to MgO. According to the Bader charge transfer analysis and the CCD plot (see Figure 2a) the H₂O molecule is a strong electron acceptor to the cluster with $\Delta q = -1.122 e$ (see Table S1 in Supporting Information). The basicity of the MgO cluster facilitates the electrons transfer from the O atom of the cluster to the H₂O molecule, while a higher electronegativity of the O atom of the

molecule facilitates electron depletion towards H atoms. Such significant charge redistribution between the MgO cluster and the H₂O contributes to its adsorption.³⁶

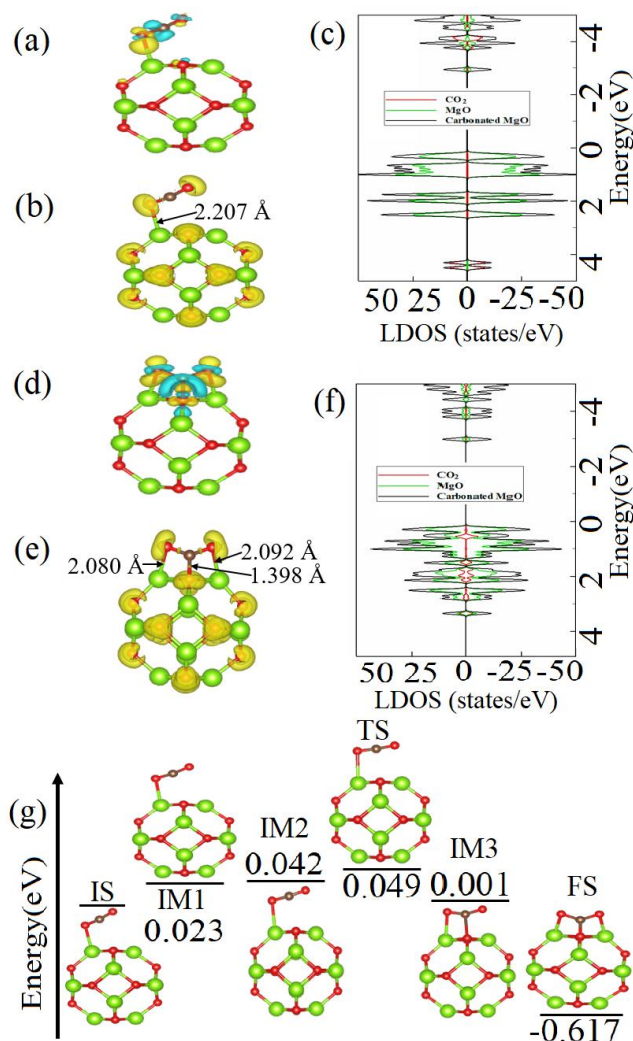


Figure 1. (a) The lowest-energy configuration of the CO₂ molecule physisorbed on the MgO cluster combined with the CDD isosurface plot (0.003 Å⁻³). (b) The ELF and (c) DOS and LDOS for the CO₂-physisorbed MgO cluster. (d) The lowest-energy configuration of the CO₂ molecule chemisorbed on the MgO cluster combined with the CDD isosurface plot (0.009 Å⁻³). (e) The ELF and (f) DOS and LDOS for the CO₂-chemisorbed MgO cluster. (g) The energy barrier and atomic structures corresponding to the minimum energy pathway for the chemisorption process of the CO₂ molecule on the MgO cluster.

The ELF plot in Figure 2b shows the electron localization between the O atom of the H₂O molecule and the Mg atom of the MgO cluster, as well as the localization between the H atom of the H₂O molecule and the O atom of the MgO cluster, which confirms electron depletions at these sites and suggests the formation of the H-O and Mg-O bonds between the molecule and the cluster. The DOS and LDOS plots in Figure 2c display the hybridization of H₂O and MgO states at -3.3 eV and 4.9 eV and a weak interaction at 4.4 eV. The conducted AIMD simulation also confirms the dissociation of the H₂O molecule on the MgO cluster and formation of the H-O and Mg-O bonds (see Movie 2 and Figure S4 in Supporting Information).

NEB calculations are carried out to show the possible reaction mechanism of the H₂O molecule dissociation on the MgO cluster. Figure 2d presents the energy profile and related atomic configurations for the IS, TS, IMs and FS showing the dissociation of the H₂O molecule of the MgO

cluster. As it is seen, between IS and TS the H₂O molecule bonding to the MgO cluster through the rotation of the H atom of the molecule (IM1). E_b of the H₂O molecule dissociation on the MgO cluster at TS is found to be as high as 0.245 eV (see Table S2 in Supporting Information). Further reaction at IM2 and IM3 leads to the bonding of the H atom of the H₂O molecule to the nearest O atom of the cluster and the consequent H₂O dissociation at FS occurring with an energy release of 0.179 eV. A higher energy release during the carbonation (-0.617 eV) of the MgO cluster compared to that during hydration (-0.179 eV) of the MgO cluster, indicates that the carbonation of the MgO cluster is a more exothermic process than its hydration. Therefore, the carbonated MgO is more thermodynamically stable. However, E_b for carbonation of the MgO cluster is 0.235 eV, which is lower than E_b of 0.245 eV for hydration of the MgO cluster. On the other hand, AIMD simulations suggest that the hydration of the MgO cluster passes faster than its carbonation (see Figure S4 in Supporting Information). Therefore, hydration and carbonation rates of the MgO cluster are compared based on the Arrhenius equation (Eq. 3), according to which the reaction rate depends on two factors: activation energy of the reaction and pre-exponential factor A. Therefore, besides the calculated E_b , the A factor, describing the frequency of collisions between reactant molecules at a standard concentration, should be taken into consideration for the comparison of hydration and carbonation rates of the MgO cluster. The hydrolysis of the MgO cluster changes its structure due to a break of Mg-O bonds of the MgO cluster upon interaction with H₂O, while the carbonation of the MgO cluster does not cause the alteration of the MgO cluster. This leads to a significant difference in the A factor for the hydration and carbonation of the cluster. As a result, the hydration of the MgO cluster is faster than its carbonation as it is shown by AIMD simulations (see Figure S4 and Movies 1 and 2 in Supporting Information). This observation is also in line with the fact that E_{ads} of the H₂O molecule (-0.95 eV) on the MgO cluster is more than 2 times lower than that of the CO₂ molecule (-0.42 eV) on the MgO cluster, which leads to faster hydration reaction. Faster hydration of the MgO cluster is also observed in AIMD simulations (see Figures S4 in Supporting Information) where the adsorption of the H₂O molecule of the MgO cluster occurs ~3 times faster than that of the CO₂ molecule. Furthermore, to compare the hydration and the carbonation rate of the MgO cluster, AIMD simulations are performed to simulate a CO₂- and H₂O-saturated environment, consisting of three CO₂ and three H₂O molecules (see Movie 3 in Supporting Information). The trajectory of these molecules shows that hydration of MgO is significantly faster than its carbonation (see Figure S5 in Supporting Information), as all three considered H₂O molecules bond to the MgO cluster before any of the CO₂ molecules.

In summary, the formation of the H-O and Mg-O bonds between the H₂O molecule and the MgO cluster verifies H₂O chemisorption on the cluster. The calculated NEB energy profile diagram predicts that the H₂O molecule dissociation on the MgO cluster is an exothermic process, and the carbonation of MgO is thermodynamically more favourable than its hydration. However, although the calculated E_b for the hydration of the MgO cluster is higher than that for its carbonation, the hydration of the MgO cluster is found to be faster, as confirmed by the calculated E_{ads} and AIMD simulations.

As it is found that hydration of MgO occurs faster than its carbonation, the CO₂ molecule interaction with the hydrated MgO cluster (previously found lowest-energy configuration of hydrated MgO is used) is studied. Several possible configurations of the CO₂ molecule on the hydrated MgO cluster are considered (see Figure S6 in Supporting Information). Figure 3a shows the lowest-energy configuration of the CO₂ molecule on the hydrated MgO cluster, where the O atom of the CO₂ molecule is bonded to the Mg atom of the MgO cluster. The newly formed Mg-O bond has a length of 2.175 Å. The length of the C-O bond (the one closest to the cluster) of the adsorbed CO₂ is elongated to 1.182 Å compared to that of bare CO₂ of 1.174 Å, while another C-O bond of CO₂

shortens to 1.165 Å. The $\angle(\text{O}-\text{C}-\text{O})$ angle of the CO_2 molecule also decreases from 179.95° to 174.43° upon its adsorption.

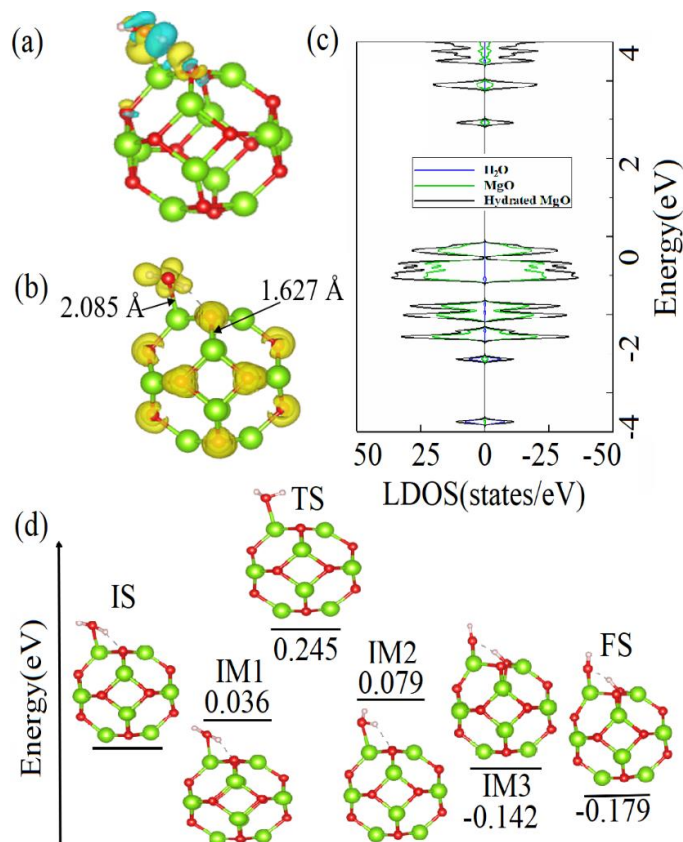


Figure 2. (a) The lowest-energy configuration of the H_2O molecule on the MgO cluster combined with the CDD isosurface plot (0.003 \AA^{-3}). (b) The ELF and (c) DOS and LDOS for the H_2O -adsorbed MgO cluster. (d) The energy barrier and atomic structures corresponding to the minimum energy pathway for the hydration of the MgO cluster.

The CDD plot in Figure 3a shows that the CO_2 molecule is an acceptor to the hydrated MgO cluster as there is a depletion of the electron on the Mg atom of the cluster and accumulation of electrons on the O atom of the CO_2 molecule. The Bader charge transfer analysis predicts that the amount of the charge transferred from the cluster to the molecule is $0.058 e$. Importantly, E_{ads} of the CO_2 molecule on the hydrated MgO cluster is -0.53 eV , which is lower than that of the CO_2 molecule on the bare MgO cluster. This suggests stronger bonding of the CO_2 molecule with the hydrated MgO cluster compared to the bare MgO cluster. The ELF plot in Figure 3b demonstrates the electron localization between the O atom of the molecule and the Mg atom of the cluster. It verifies the accumulation of electrons on the O atoms of the CO_2 molecule and suggests that the $\text{C}-\text{O}$ bonds of the molecule remain covalent. The DOS and LDOS plots in Figure 3c show strong overlapping of HOMO states of the H_2O molecule and the MgO cluster in the range from -4.2 to -4.8 eV and strong overlapping of LUMO+1 states of the H_2O molecule and the MgO cluster in the range from 3.4 to 4.5 eV , which confirms a strong bonding between the CO_2 molecule and the hydrated MgO cluster. The conducted AIMD calculations predict the possibility of chemisorption of the CO_2 molecule on the hydrated MgO cluster at room temperature. In chemisorbed state, the O atoms of the CO_2 molecule are bonded to the Mg atoms of the hydrated MgO cluster and the C atom of the CO_2 molecule is bonded to the O atom of the hydrated MgO cluster (see Movie 4 and Figure S7 in Supporting Information). It is observed that the carbonation of bare MgO occurs slower than the carbonation of

hydrated MgO due to the formation of OH groups on the MgO cluster during its hydration, that hinder the carbonation process.

To gain insights into the carbonation mechanism of hydrated MgO, the chemisorption process of CO₂ on it is considered. The lowest-energy configuration of chemisorbed CO₂ molecule on the hydrated MgO cluster (for more details see Figure S7 in Supporting Information) is shown in Figure 3d. Here, both O atoms of the CO₂ molecule form chemical bonds with the Mg atoms of the hydrated MgO cluster. The C–O bonds of the CO₂ molecule are elongated to 1.269 Å and 1.275 Å (compared to 1.174 Å of the bare CO₂ molecule) upon its adsorption on the hydrated MgO cluster. The length of newly formed Mg–O bonds is 2.057 Å and 2.025 Å, while the length of the C–O bond formed between the C atom of the molecule and the O atom of the cluster is 1.382 Å. The ∠(O–C–O) angle of the adsorbed CO₂ molecule is found to be 129.16°, which is lower than that of the CO₂ molecule in its physisorbed state. The CDD plot in Figure 3d shows that the charge is mostly distributed on the CO₂ molecule and partially on the O atom of the MgO cluster bonded to the C atom of the CO₂ molecule. The basicity of the hydrated MgO cluster drives the electron transfer from the molecule to the hydrated cluster. According to the Bader charge transfer analysis, the chemisorbed CO₂ molecule gains 0.086 *e* from the hydrated MgO cluster. Therefore, the amount of the charge transferred from the hydrated MgO cluster to the chemisorbed CO₂ molecule is higher than that from the hydrated MgO cluster to the physisorbed CO₂ molecule (see Table S1 Supporting Information). The calculated *E*_{ads} of -1.55 eV for the CO₂ molecule chemisorbed on the hydrated MgO cluster is higher than that of the CO₂ molecule chemisorbed on the bare MgO cluster (-1.05 eV). The ELF plot in Figure 3e depicts electron localizations between the O atoms of the chemisorbed CO₂ molecule and the Mg atoms of the hydrated MgO cluster and the C atom of the chemisorbed CO₂ molecule and the O atom of the hydrated MgO cluster, which suggests the existence of the covalent Mg–O and C–O bonds between the cluster and the molecule. Meanwhile, the covalent bonding between the H₂O molecule and the MgO cluster remains unchanged. According to DOS and LDOS plots presented in Figure 3f, there is a strong hybridization of HOMO and HOMO-1 states of the hydrated MgO cluster and the chemisorbed CO₂ molecule. The overlapping of the cluster and the molecule is also observed at -3.8 eV, -4.5 eV and 4.6 eV.

*E*_b of 0.275 eV (see Table S2 in Supporting Information) for the transition of the CO₂ molecule from physisorbed state to chemisorbed state on the hydrated MgO cluster is calculated by the NEB approach (see Figure 3g). The transition involves the IM2 stage, where the O atom of the CO₂ molecule oxidizes the Mg atom of the MgO cluster, which leads to the drop of *E*_b to 0.153 eV. This triggers an exothermic process of bonding the C and O atoms of the CO₂ molecule to the hydrated MgO cluster at the FS state via the IM3 (-0.800) state with the released energy of 1.028 eV. According to calculated reaction energies in the carbonation process of bare MgO (-0.617 eV) and hydrated MgO (-1.028 eV), carbonation of the hydrated MgO is thermodynamically more favourable. However, *E*_b for the transition of CO₂ from the physisorbed state to the chemisorbed state on hydrated MgO (0.275 eV) is higher than that of CO₂ on bare MgO (0.234 eV). Therefore, CO₂ chemisorption on hydrated MgO is kinetically unfavourable. This matches the AIMD simulation results (see Figures S2 and S6 in Supporting Information), where the carbonation of bare MgO is faster than that of the hydrated MgO. Importantly, this verifies the fact that the initial hydration of MgO can hinder its carbonation.¹⁵

In summary, the chemisorption of the CO₂ on the MgO cluster is found to be the most energetically favourable. The charge redistribution between the MgO cluster and the CO₂ molecule during the chemisorption^{37,38} and the comparison of the energy released during carbonation of the bare and the hydrated MgO clusters suggests carbonation of the bare MgO cluster is faster than that of the hydrated MgO cluster, which uncovers the hindrance effect of H₂O on the carbonation of MgO.

The observed results are also supported by AIMD simulations (see Movie 4 and Figure S7 in Supporting Information).

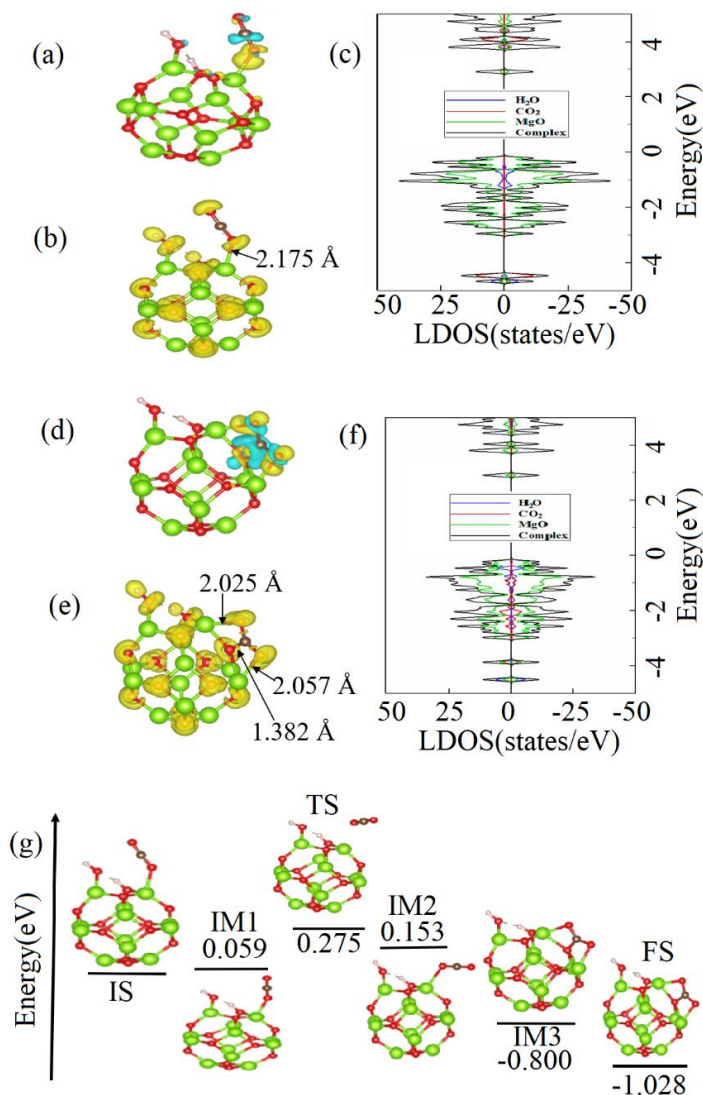


Figure 3. (a) The lowest-energy configuration of the physisorbed CO_2 molecule on the hydrated MgO cluster combined with the CDD isosurface plot (0.003 \AA^{-3}). (b) The ELF and (c) DOS and LDOS for the CO_2 -physisorbed hydrated MgO cluster. (d) The lowest-energy configuration of the chemisorbed CO_2 molecule on the hydrated MgO cluster combined with the CDD isosurface plot (0.009 \AA^{-3}). (e) The ELF and (f) DOS and LDOS for the CO_2 -chemisorbed hydrated MgO cluster. (g) The energy barrier and atomic structures corresponding to the minimum energy pathway for the transition of the CO_2 molecule from physisorbed to chemisorbed states on the hydrated MgO cluster.

Mg(OH)₂ interaction with CO₂ and H₂O. In RMC reactions, the carbonation of Mg(OH)_2 leads to the production of a range of HMCs.^{12,13} Therefore, the mechanism of the carbonation of Mg(OH)_2 is further studied. For that, several possible configurations of the CO_2 molecule and the Mg(OH)_2 cluster are examined (see Figure S8 in Supporting Information). The most favourable sites for the CO_2 molecule adsorption on Mg(OH)_2 are located at its edges. Figure 4a combines the atomic structure of the lowest-energy configuration and the CDD plot for the CO_2 molecule adsorbed on the Mg(OH)_2 cluster. In that case, the C atom of the CO_2 molecule is located below the O atom at the edge of the Mg(OH)_2 cluster and is bonded to the O atom of the cluster. In the same way, the O atom of the CO_2 molecule is bonded to the Mg atom at the edge of the Mg(OH)_2 cluster and forms the Mg–O bond of a length of 2.069 \AA . Upon adsorption, the C–O bonds in the CO_2 molecule elongates from 1.174 \AA

(bare CO₂) to 1.266 Å, while a newly formed C–O bond between the CO₂ molecule and Mg(OH)₂ has a length of 1.515 Å and ∠(O–C–O) changes from 179.95° to 136.88°. The CDD plot in Figure 4a displays the charge transfer from O atoms at the edge of Mg(OH)₂ to the CO₂ molecule. The Bader charge transfer analysis suggests that CO₂ acts as an acceptor to the Mg(OH)₂ cluster, with the charge transfer from the cluster to the molecule of 0.397 *e* (see Table S1 in Supporting Information). This verifies the Lewis basicity of the Mg(OH)₂ cluster. According to Table S1 (see Supporting Information), the *E*_{ads} of CO₂ on Mg(OH)₂ is -0.69 eV.

The ELF plot in Figure 4b shows electron localization between the O atom of the CO₂ molecule and the Mg atom of the Mg(OH)₂ cluster, which characterizes electron transfer and strong bonding between the molecule and the edge of the cluster. The covalent bonding within the molecule also remains stable, as predicted by the charge localization on both the C–O bonds of the CO₂ molecule. The DOS and LDOS plots for the CO₂-adsorbed Mg(OH)₂ cluster are shown in Figure 4c. The observed strong orbital hybridisation of CO₂ and Mg(OH)₂ at the energy of -1.7 eV and in a range from -2 to -3.7 eV confirms the strong interaction between CO₂ and Mg(OH)₂ proposed by the charge transfer and ELF analysis. Figure 4d depicts the potential energy profile and atomic structures corresponding to the minimum energy pathway for the carbonation of the Mg(OH)₂ cluster. It is shown that *E*_b for the carbonation of Mg(OH)₂ is as low as 0.002 eV (TS in Figure 4d), which is equivalent to a spontaneous process at room temperature. To reach the chemisorbed state at FS (-0.303 eV), the CO₂ molecule passes through the IM2 state (-0.064 eV) where the C atom of the molecule bonds to the O atom of the cluster, and IM3 (-0.256), at which point the O atom of the molecule forms a bond with the Mg atom of the cluster. It is also noted that the carbonation of Mg(OH)₂ is a highly exothermic process.

In summary, the elongation of C–O bonds and the decrease of ∠(O–C–O) of the CO₂ molecule, along with the strong charge transfer between the molecule and the Mg(OH)₂ cluster, play a dominant role in CO₂ chemisorption on Mg(OH)₂. Despite the chemisorption of CO₂ on Mg(OH)₂ occurring only at the edges, chemisorption mechanism of CO₂ for Mg(OH)₂ is similar to that for MgO. In both cases, chemisorption of CO₂ is an exothermic process with low *E*_b and significant energy release. However, the activation energy for the carbonation of Mg(OH)₂ (0.002 eV) is significantly lower than that for MgO (0.049 eV), confirming that carbonation of the Mg(OH)₂ is faster than that of the MgO. In turn, the energy released during the MgO carbonation (-0.617 eV) is about 2 times lower than that during the Mg(OH)₂ carbonation (-0.303 eV), which suggests that the carbonation of the MgO cluster is more thermodynamically favourable.

Mg(OH)₂ is often affected by aqueous environments, therefore, the interaction of the H₂O molecule with the Mg(OH)₂ cluster can play a key role in HMC formation. From the studied configurations for that interaction of H₂O with Mg(OH)₂ (see Figure S9 in Supporting Information), the lowest-energy configuration is related to the H₂O molecule located at the edge of the Mg(OH)₂ cluster. The length of the O–H bond of the bare H₂O molecule (1.972 Å) is shortened to 1.020 Å upon the H₂O molecule bonding to the Mg(OH)₂ cluster, while the O–H bond at the edge of the Mg(OH)₂ cluster is elongated from 0.965 Å to 0.984 Å. The CDD plot in Figure 4e shows that the charge is mostly distributed on the H₂O molecule and partially at the edge of the Mg(OH)₂ cluster. The Bader charge transfer analysis predicts the H₂O molecule to be a weak acceptor to the Mg(OH)₂ cluster that accumulates 0.044 *e* (see Table S1 in Supporting Information). *E*_{ads} of the H₂O molecule on the Mg(OH)₂ cluster is -0.74 eV (see Table S1 in Supporting Information). The ELF plot in Figure 4f shows insignificant electron distributions between the O atom of the H₂O molecule and the H atom of the Mg(OH)₂ cluster. Meanwhile, low electron density between the H atom of the H₂O molecule and the O atom of the Mg(OH)₂ cluster indicates weak interaction between them. Moreover, orbital localization between the O–H bonds of the H₂O molecule shows that the covalent bonds of the

molecule remain stable. The DOS and LDOS plots for the H₂O molecule adsorbed on the Mg(OH)₂ cluster, shown in Figure 4g, also suggests a weak interaction between the molecule and the cluster at -1.5 eV, -1.8 eV, -2 eV, and in ranges from -2.2 to -2.5 eV and from -4.1 to -4.2 eV.

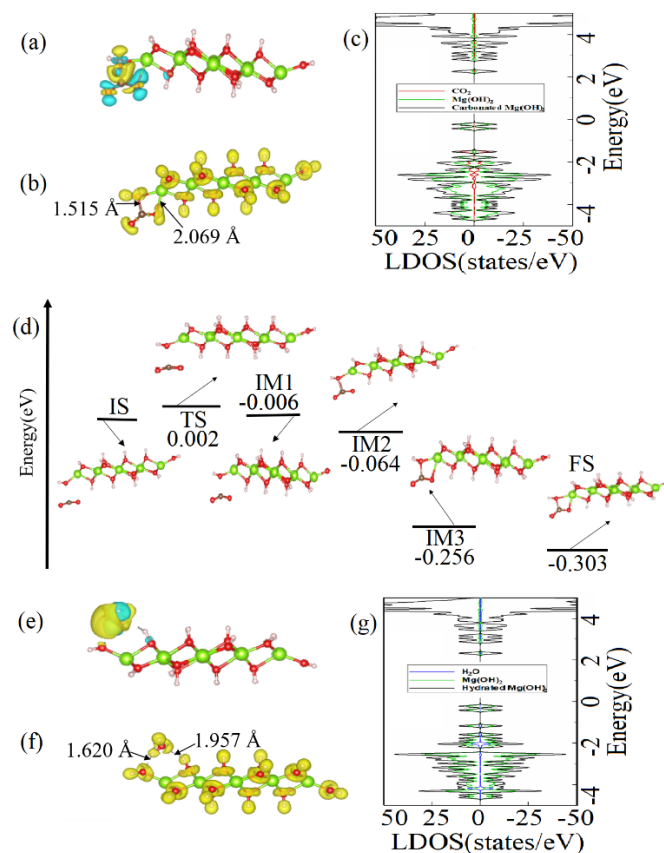


Figure 4. (a) The atomic structure of the lowest-energy configuration of the CO₂ molecule on the Mg(OH)₂ cluster combined with the CDD isosurface plot (0.006 Å⁻³). (b) The ELF and (c) DOS and LDOS for the CO₂-adsorbed Mg(OH)₂ cluster. (d) The energy barrier and atomic structures corresponding to the minimum energy pathway for the carbonation of the Mg(OH)₂ cluster. (e) The atomic structure of the lowest-energy configuration of the H₂O molecule on the Mg(OH)₂ cluster combined with the CDD isosurface plot (0.009 Å⁻³). (f) The ELF and (g) DOS and LDOS for the H₂O-adsorbed Mg(OH)₂ cluster.

In summary, it is found that the H₂O molecule is located at the edges of the Mg(OH)₂ cluster. The calculated low E_{ads} and weak charge transfer between the H₂O molecule and the Mg(OH)₂ cluster suggest that H₂O is physisorbed on Mg(OH)₂. However, it is well-known that the presence of H₂O facilitates the formation of HMCs in accessible pores during the carbonation process.³⁷

To investigate a mechanism of reaction of nesquehonite formation (Mg(OH)₂ + CO₂ + 2H₂O → MgCO₃·3H₂O), at the first step, the simultaneous interaction of the carbonated Mg(OH)₂ cluster and the H₂O molecule (Mg(OH)₂ + CO₂ + H₂O) is considered. At the second step, one more H₂O molecule is introduced to the system studied at the first step (CO₂ + 2H₂O + Mg(OH)₂). Although the natural process of the nesquehonite formation also includes nucleation and growth from species in solution, the studied reaction will still help to understand possible nucleation or growth paths of nesquehonite. At the first step, various configurations of one H₂O molecule (see Figure S10 in Supporting Information) on the carbonated Mg(OH)₂ cluster are considered. At the lowest-energy configuration, the H₂O molecule is bonded to the edge of the Mg(OH)₂ cluster. The length of the O–

H bonds increases to 0.970 Å and 1.022 Å compared to these of the bare H₂O molecule (0.936 Å). The distance between the H atom of the H₂O molecule and the O atom of the Mg(OH)₂ cluster is 1.620 Å, while the distance between the O atom of the H₂O and the H atom of the Mg(OH)₂ cluster is 1.957 Å. According to Table S1 (see Supporting Information), E_{ads} of the H₂O molecule on the Mg(OH)₂ cluster is -0.86 eV. The CDD plot in Figure 5a shows that there is a depletion of electrons at the edge O atoms of the Mg(OH)₂ cluster and charge accumulation at the H atoms of the H₂O molecule. The Bader charge transfer analysis shows that the H₂O molecule gains 0.046 e from the Mg(OH)₂ cluster which confirms that H₂O is a weak acceptor to Mg(OH)₂ (see Table S1 in Supporting Information). Further, the ELF plot in Figure 5b shows H₂O is physisorbed on Mg(OH)₂, as there is no electron density localization between the Mg(OH)₂ cluster and the H₂O molecule, while the H-O bonds of H₂O remain their covalent nature. Figure 5c represents the DOS and LDOS plots for the H₂O molecule adsorption on the carbonated Mg(OH)₂ cluster. Small overlapping of states of the H₂O molecule and the carbonated Mg(OH)₂ cluster is observed in the range from -3.0 to -3.7 eV, verifying weak interaction between them.

Further, at the second step, the second H₂O molecule is introduced to the Mg(OH)₂ + CO₂ + H₂O system obtained at the first step (see Figure S11 in Supporting Information). The lowest energy configuration of the H₂O molecule on the Mg(OH)₂ + CO₂ + H₂O system is shown in Figure 5d, where the second H₂O molecule is also located at the edge of the carbonated Mg(OH)₂ cluster. The length of the H-O bonds of the bare H₂O molecule is 0.971 Å, while they slightly elongate to 0.975 Å and 0.973 Å after adsorption. The distance between the O atom of the H₂O molecule and the Mg atom of the Mg(OH)₂ cluster is 2.232 Å. According to Table S1 (see Supporting Information) E_{ads} of the H₂O molecule on the Mg(OH)₂ + CO₂ + 2H₂O system is -0.46 eV. The CDD plot in Figure 5d displays the depletion of electrons at O atoms located at the edge of the Mg(OH)₂ cluster and charge accumulation at the H atoms of the H₂O molecule. According to the Bader charge transfer analysis (see Table S1 in Supporting Information) the H₂O molecule is a weak acceptor to the Mg(OH)₂ cluster with the charge transfer of 0.037 e from the cluster to the molecule. The ELF plot in Figure 5e shows no electron density localization between the second H₂O molecule and the Mg(OH)₂ + CO₂ + H₂O system, which means there is a weak interaction between them. The DOS and LDOS plots in Figure 5f also display a weak interaction of the H₂O molecule and the cluster at the range from -2.8 to -3.5 eV.

AIMD simulations are used to investigate the reaction for the formation of HMCs via the interaction of the CO₂ and H₂O molecules with the Mg(OH)₂ cluster (see Movie 5 and Figures 5g and h in Supporting Information.). As it is shown, the CO₂ and H₂O molecules are bonded at the edges of the Mg(OH)₂ cluster, which suggests that the formation of HMCs starts at the edges of Mg(OH)₂. Further, AIMD simulations are conducted to consider the effect of large amount of H₂O and CO₂ molecules on the formation of HMCs (see Movie 6 in Supporting Information). For that, two H₂O and one CO₂ molecules are added to the previously considered Mg(OH)₂ + CO₂ + 2H₂O system. As shown in Figure 5h, the first CO₂ molecule is able to carbonate the Mg(OH)₂ cluster. However, after the bonding of the first CO₂ molecule to the cluster, the second CO₂ molecule is unable to bind to the carbonated Mg(OH)₂ cluster (Figures 5i and j). This suggests that the formation of an early layer of carbonates in RMC-based concrete formulations may limit the continuation of carbonation by forming a physical barrier that prohibits further interaction between Mg(OH)₂ and CO₂. These limitations in carbonation of Mg(OH)₂ can cause large amounts of unreacted crystals leading to relatively low strength and porous microstructures.^{15,43} Although the presence of H₂O molecules provides the medium for carbonation and further transformation of Mg(OH)₂ into HMCs and is required for the continuous formation of HMCs⁴⁴, according to the AIMD simulations, excessive H₂O hinders CO₂ penetration to the Mg(OH)₂ surface. Therefore, to maintain CO₂ diffusion for

carbonation of $\text{Mg}(\text{OH})_2$, the amount of H_2O should be properly controlled.⁴⁰ The predicted results of $\text{Mg}(\text{OH})_2$ passivation with the formation of the barrier of carbonates and H_2O hindrance effect on carbonation of MgO correspond to the carbonation mechanisms of portlandite.⁴⁵

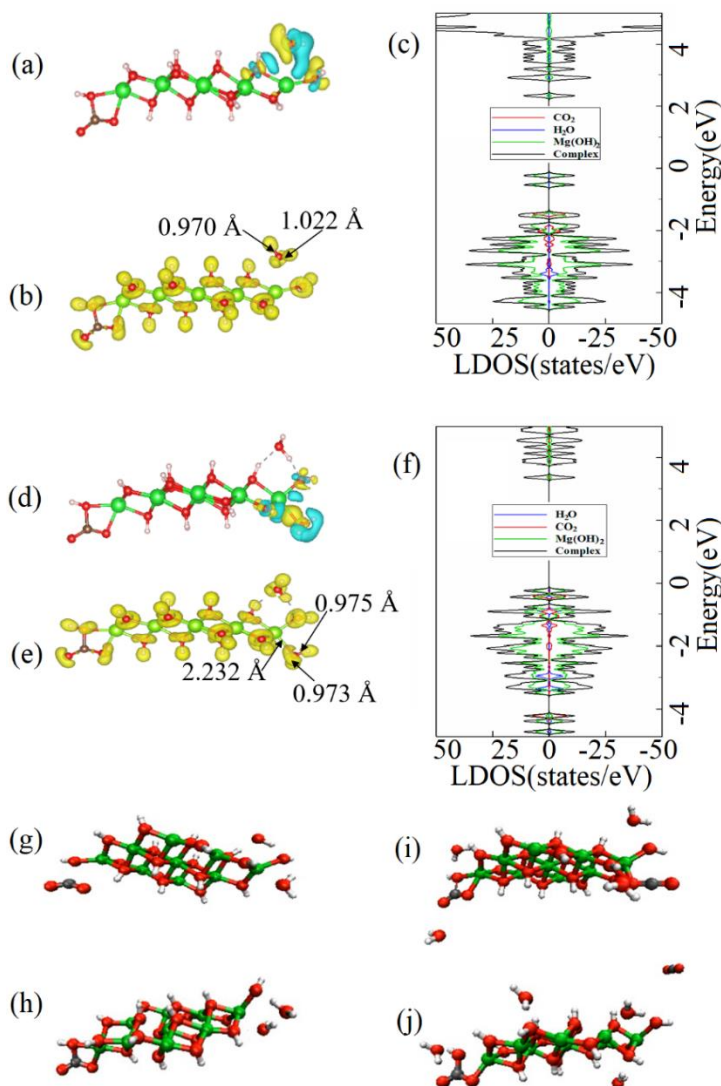


Figure 5. (a) The lowest-energy configuration of the H_2O molecule on the carbonated $\text{Mg}(\text{OH})_2$ cluster with the CDD isosurface plot (0.001 \AA^{-3}). (b) The ELF and (c) DOS and LDOS for H_2O molecules on the carbonated $\text{Mg}(\text{OH})_2$ cluster. (d) The lowest-energy structure of the H_2O molecules on the carbonated $\text{Mg}(\text{OH})_2$ cluster combined with the CDD plot (0.001 \AA^{-3}). (e) The ELF and (f) DOS and LDOS for the H_2O molecule on the carbonated $\text{Mg}(\text{OH})_2$ cluster. (g) Initial and (h) final (chemisorbed state) configurations of CO_2 and H_2O molecules on the $\text{Mg}(\text{OH})_2$ cluster. (i) Initial and (j) final configurations of CO_2 and H_2O molecules on the carbonated $\text{Mg}(\text{OH})_2$ cluster.

As the adsorption behaviour of molecules on the clusters may be different from that on the bulk materials. Further, the interaction of the CO_2 and H_2O molecules with clusters and with the bulk MgO and $\text{Mg}(\text{OH})_2$ is compared. Figures 6a and b represent the lowest-energy configuration of the CO_2 and H_2O molecules on $\text{MgO}(001)$. Figure 6a shows the O atom of CO_2 molecule is located above Mg atom of $\text{MgO}(001)$. The length of C–O bonds in the CO_2 molecule elongates from 1.174 \AA (bare CO_2) to 1.182 \AA and 1.175 \AA and $\angle(\text{O}–\text{C}–\text{O})$ decreases from 179.95° to 176.81°. The calculated E_{ads} for CO_2 on the $\text{MgO}(001)$ surface is -0.34 eV (see Table S3 in Supporting Information). This indicates weak adsorption of CO_2 on the bulk $\text{MgO}(001)$ compared to the physisorbed- CO_2 on the MgO cluster ($E_{\text{ads}} = -0.42$ eV). According to Figure 6b, O atom of H_2O molecule is located above Mg atom of $\text{MgO}(001)$. The length of the H–O bonds of the H_2O molecule,

elongates from 0.972 Å (bare H₂O) to 0.983 Å and 0.977 Å. $E_{\text{ads}} = -0.58$ eV of the H₂O molecule on MgO(001) (see Table S3 in Supporting Information) is found to be lower than that of the H₂O molecule (-0.95 eV) on the MgO cluster. The length of the Mg–O bond formed between the O atom of the H₂O molecule and the Mg atom at the MgO(001) surface is 2.239 Å, which is longer than the Mg–O bond formed between the O atom of the H₂O molecule and the Mg atom of the MgO cluster (2.085 Å). Therefore, for both H₂O and CO₂ molecules their adsorption and possible dissociation at the edges or defective surfaces of the MgO crystal, presented here via clusters, is more favourable. This result well matches the previously reported observation on weak adsorption of the CO₂ molecule on the MgO(001) surface.²⁴

Figures 6c and d show the lowest-energy configurations of the CO₂ and H₂O molecules on the Mg(OH)₂(001) surface. Figure 6c indicates the location of the C atom of the CO₂ molecule is located above the Mg–O bond of the Mg(OH)₂(001) surface. The C–O bonds in the CO₂ molecule elongates from 1.174 Å (bare CO₂) to 1.177 Å and 1.178 Å, and $\angle(\text{O–C–O})$ changes from 179.95° to 179.00°. E_{ads} of the CO₂ molecule on the Mg(OH)₂(001) surface is as low as -0.25 eV, which is significantly lower than that of the CO₂ molecule on the Mg(OH)₂ cluster (-0.69 eV) (see Table S3 in Supporting Information). Figure 6d depicts interaction of the H atom of H₂O molecule with the O atom of the Mg(OH)₂(001) surface. The length of the H–O bond of the H₂O molecule near to the surface, elongates from 0.972 Å (bare H₂O) to 0.994 Å, while another O–H bond is shortened to 0.952 Å. E_{ads} of H₂O molecule on the Mg(OH)₂(001) surface is found to be -0.37 eV, which is lower than that of the H₂O molecule on Mg(OH)₂ cluster (-0.74 eV) (see Table S3 in Supporting Information). In addition, the distance between the H₂O molecule and the Mg(OH)₂(001) surface of 2.017 Å, is longer than that between the H₂O molecule and the Mg(OH)₂ cluster (1.957 Å). Similar to the case of MgO, the lower E_{ads} of the CO₂ and H₂O molecules on the Mg(OH)₂ cluster, compared to that on the Mg(OH)₂(001) surface, suggests stronger interaction of these molecules with the edge and/or defect-containing surface of Mg(OH)₂ crystal.

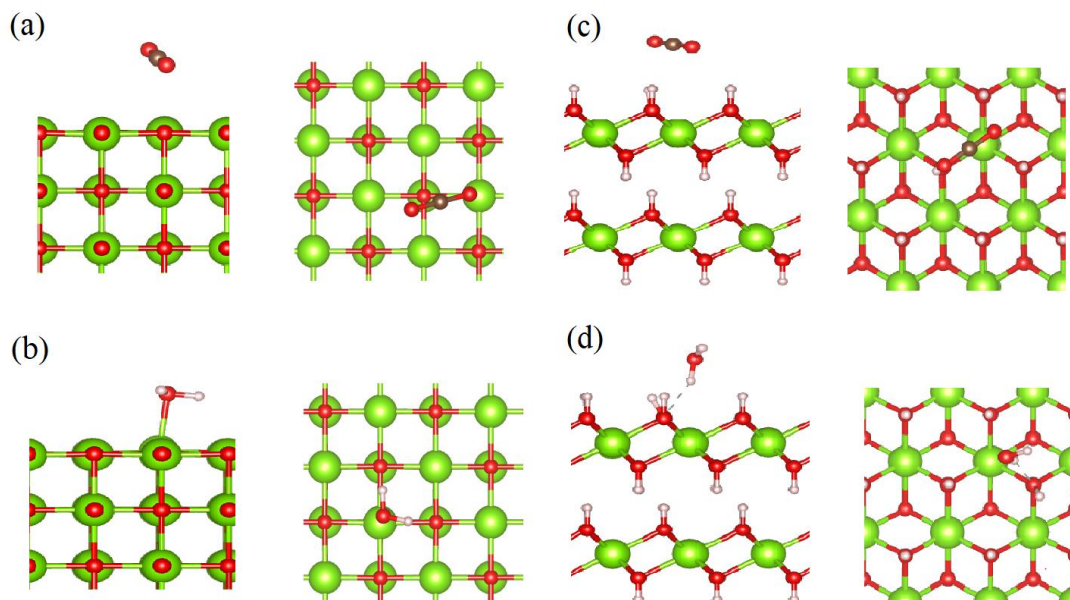


Figure 6. The side and top views of the lowest-energy configuration of (a) CO₂ and (b) H₂O molecules on the MgO(001) surface. The side and top views of the lowest-energy configuration of (c) CO₂ and (d) H₂O molecules on the Mg(OH)₂(001) surface.

Conclusions

In the present study, the mechanism of potential reactions on MgO and Mg(OH)₂ during HMC synthesis is investigated by DFT-based calculations. The results show that despite the energy barrier

for the CO₂ molecule adsorption on MgO is lower than that for the H₂O molecule adsorption on MgO, the hydration of MgO is faster, due to the difference in the frequency of CO₂ and H₂O molecules collisions with MgO. In addition, it is found that adsorption of CO₂ on hydrated MgO is slower than that on bare MgO, which means that the presence of H₂O molecules (moisture environment) can hinder MgO carbonation. In turn, the carbonation of Mg(OH)₂ is found to be significantly faster than that of MgO. It should be noted, that both hydration and carbonation of Mg(OH)₂ take place at the edges. In addition, a weaker interaction of the CO₂ and H₂O molecules with the MgO and Mg(OH)₂ surfaces compared to the edge and/or defect-containing surfaces (clusters) is found. Importantly, two limiting factors of the HMCs formation reaction are found: i) surface passivation of Mg(OH)₂ upon its initial carbonation and ii) surface covering of Mg(OH)₂ by H₂O molecules, which inhibits the carbonation on Mg(OH)₂.

Acknowledgements

M.G.G., H.N. and P.K. are grateful for the support of the Academy of Finland grant CCC (329477) and the University of Oulu and the Academy of Finland Profi5 funding (326291). K.A.A. and W.C. acknowledge funding from the European Research Council (ERC) under the European Union's Horizon 2020 research and innovation programme (grant agreement No. 101002219). H.M. would like to acknowledge funding from "Departamento de Educación, Política Lingüística y Cultura del Gobierno Vasco" (Grant No. IT1358-22). The authors wish to acknowledge CSC-IT Center for Science, Finland, for providing computational resources.

References

- (1) Kulp, S. A.; Strauss, B. H. New Elevation Data Triple Estimates of Global Vulnerability to Sea-Level Rise and Coastal Flooding. *Nat. Commun.* **2019**, *10* (1), 1–12.
- (2) Olivier, J. G. I.; Peters, J. A. H. W.; Janssens-Maenhout, G. Trends in Global CO₂ Emissions 2012 Report. **2012**.
- (3) Van Oss, H. G.; Padovani, A. C. Cement Manufacture and the Environment: Part I: Chemistry and Technology. *J. Ind. Ecol.* **2002**, *6* (1), 89–105.
- (4) Birchal, V. S. S.; Rocha, S. D. F.; Ciminelli, V. S. T. The Effect of Magnesite Calcination Conditions on Magnesia Hydration. *Miner. Eng.* **2000**, *13*, 1629–1633.
- (5) Walling, S. A.; Provis, J. L. Magnesia-Based Cements: A Journey of 150 Years, and Cements for the Future? *Chem. Rev.* **2016**, *116* (7), 4170–4204.
- (6) Gartner, E.; Sui, T. Alternative Cement Clinkers. *Cem. Concr. Res.* **2018**, *114*, 27–39.
- (7) Ruan, S.; Unluer, C. Comparative Life Cycle Assessment of Reactive MgO and Portland Cement Production. *J. Clean. Prod.* **2016**, *137*, 258–273.
- (8) Zhongming, Z.; Linong, L.; Wangqiang, Z.; Wei, L. AR6 Climate Change 2021: The Physical Science Basis. **2021**.
- (9) Unluer, C.; Al-Tabbaa, A. Impact of Hydrated Magnesium Carbonate Additives on the Carbonation of Reactive MgO Cements. *Cem. Concr. Res.* **2013**, *54*, 87–97.
- (10) Li, X. Mechanical Properties and Durability Performance of Reactive Magnesia Cement Concrete. University of Cambridge 2013.
- (11) Ma, S.; Akca, A. H.; Esposito, D.; Kawashima, S. Influence of Aqueous Carbonate Species on Hydration and Carbonation of Reactive MgO Cement. *J. CO₂ Util.* **2020**, *41*, 101260.
- (12) Unluer, C.; Al-Tabbaa, A. Enhancing the Carbonation of MgO Cement Porous Blocks through Improved Curing Conditions. *Cem. Concr. Res.* **2014**, *59*, 55–65.
- (13) Thomas, J. J.; Musso, S.; Prestini, I. Kinetics and Activation Energy of Magnesium Oxide Hydration. *J. Am. Ceram. Soc.* **2014**, *97* (1), 275–282.
- (14) Matabola, K. P.; van der Merwe, E. M.; Strydom, C. A.; Labuschagne, F. J. W. The Influence of Hydrating Agents on the Hydration of Industrial Magnesium Oxide. *J. Chem.*

- Technol. Biotechnol.* **2010**, 85 (12), 1569–1574.
- (15) Dung, N. T.; Unluer, C. Development of MgO Concrete with Enhanced Hydration and Carbonation Mechanisms. *Cem. Concr. Res.* **2018**, 103, 160–169.
 - (16) Zhao, J.; Huang, X.; Shi, R.; Tang, L.; Su, Y.; Sai, L. Ab Initio Global Optimization of Clusters. *Chem. Model.* **2015**, 12, 249–292.
 - (17) Kistanov, A. A.; Shcherbinin, S. A.; Ustiuzhanina, S. V.; Huttula, M.; Cao, W.; Nikitenko, V. R.; Prezhdo, O. V. First-Principles Prediction of Two-Dimensional B3C2P3 and B2C4P2: Structural Stability, Fundamental Properties, and Renewable Energy Applications. *J. Phys. Chem. Lett.* **2021**, 12 (13), 3436–3442.
 - (18) Liu, B.; Zhou, K. Recent Progress on Graphene-Analogous 2D Nanomaterials: Properties, Modeling and Applications. *Prog. Mater. Sci.* **2019**, 100, 99–169.
 - (19) Alessio, M.; Usvyat, D.; Sauer, J. Chemically Accurate Adsorption Energies: CO and H₂O on the MgO (001) Surface. *J. Chem. Theory Comput.* **2018**, 15 (2), 1329–1344.
 - (20) Fan, H.-X.; Cui, T.-Y.; Rajendran, A.; Yang, Q.; Feng, J.; Yue, X.-P.; Li, W.-Y. Comparative Study on the Activities of Different MgO Surfaces in CO₂ Activation and Hydrogenation. *Catal. Today* **2020**, 356, 535–543.
 - (21) Huang, J.; Li, X.; Wang, X.; Fang, X.; Wang, H.; Xu, X. New Insights into CO₂ Methanation Mechanisms on Ni/MgO Catalysts by DFT Calculations: Elucidating Ni and MgO Roles and Support Effects. *J. CO₂ Util.* **2019**, 33, 55–63.
 - (22) Jang, J. M.; Kang, S. G. Understanding CO₂ Adsorption on a M1 (M₂)-Promoted (Doped) MgO–CaO (100) Surface (M₁= Li, Na, K, and Rb, M₂= Sr): A DFT Theoretical Study. *ACS Sustain. Chem. Eng.* **2019**, 7 (20), 16979–16984.
 - (23) Cornu, D.; Guesmi, H.; Krafft, J.-M.; Lauron-Pernot, H. Lewis Acido-Basic Interactions between CO₂ and MgO Surface: DFT and DRIFT Approaches. *J. Phys. Chem. C* **2012**, 116 (11), 6645–6654.
 - (24) Wu, S.; Tan, B. T.; Senevirathna, H. L.; Wu, P. Polarization of CO₂ for Improved CO₂ Adsorption by MgO and Mg (OH)₂. *Appl. Surf. Sci.* **2021**, 562, 150–187.
 - (25) Dung, N. T.; Lesimple, A.; Hay, R.; Celik, K.; Unluer, C. Formation of Carbonate Phases and Their Effect on the Performance of Reactive MgO Cement Formulations. *Cem. Concr. Res.* **2019**, 125, 105894.
 - (26) Hopkinson, L.; Kristova, P.; Rutt, K.; Cressey, G. Phase Transitions in the System MgO–CO₂–H₂O during CO₂ Degassing of Mg-Bearing Solutions. *Geochim. Cosmochim. Acta* **2012**, 76, 1–13.
 - (27) Castleman, A. W.; Bowen, Kh. Clusters: Structure, Energetics, and Dynamics of Intermediate States of Matter. *J. Phys. Chem.* **1996**, 100 (31), 12911–12944.
 - (28) Ohlin, C. A.; Villa, E. M.; Rustad, J. R.; Casey, W. H. Dissolution of Insulating Oxide Materials at the Molecular Scale. *Nat. Mater.* **2010**, 9 (1), 11–19.
 - (29) Kresse, G.; Furthmüller, Efficient Iterative Schemes For Ab Initio Total-Energy Calculations Using a Plane-Wave Basis Set. *J. Phys. Rev. B: Condens. Matter Mater. Phys.* **1996**, 54, 11169–11186.
 - (30) Blöchl, P. E. Projector Augmented-Wave Method. *Phys. Rev. B* **1994**, 50 (24), 17953.
 - (31) Perdew, J. P.; Burke, K.; Ernzerhof, M. Generalized Gradient Approximation Made Simple. *Phys. Rev. Lett.* **1996**, 77 (18), 3865.
 - (32) Zhang, S.; Zhang, Y.; Huang, S.; Liu, H.; Wang, P.; Tian, H. Theoretical Investigation of Growth, Stability, and Electronic Properties of Beaded ZnO Nanoclusters. *J. Mater. Chem.* **2011**, 21 (42), 16905–16910.
 - (33) Chen, M.; Dixon, D. A. Structure and Stability of Hydrolysis Reaction Products of MgO Nanoparticles Leading to the Formation of Brucite. *J. Phys. Chem. C* **2017**, 121 (39), 21750–21762.
 - (34) Zhang, D.; Sun, Y.; Chen, L.; Zhang, S.; Pan, N. Influence of Fabric Structure and Thickness

on the Ballistic Impact Behavior of Ultrahigh Molecular Weight Polyethylene Composite Laminate. *Mater. Des.* **2014**, *54*, 315–322.

- (35) Becke, A. D. Density-Functional Exchange-Energy Approximation with Correct Asymptotic Behavior. *Phys. Rev. A* **1988**, *38* (6), 3098.
- (36) Niu, J.; Wang, Y.; Qi, Y.; Dam, A. H.; Wang, H.; Zhu, Y.-A.; Holmen, A.; Ran, J.; Chen, D. New Mechanism Insights into Methane Steam Reforming on Pt/Ni from DFT and Experimental Kinetic Study. *Fuel* **2020**, *266*, 117143.
- (37) Richard F. W. Bader. *Bader Atoms in Molecules – A Quantum Theory*; Oxford University Press: New York, 1990.
- (38) Laidler, K. J. *Chemical Kinetics*; Harper & Row: New York, 1987.
- (39) Kistanov, A. A.; Cai, Y.; Zhou, K.; Srikanth, N.; Dmitriev, S. V.; Zhang, Y.-W. Exploring the Charge Localization and Band Gap Opening of Borophene: A First-Principles Study. *Nanoscale* **2018**, *10* (3), 1403–1410.
- (40) Henkelman, G.; Uberuaga, B. P.; Jónsson, H. A Climbing Image Nudged Elastic Band Method for Finding Saddle Points and Minimum Energy Paths. *J. Chem. Phys.* **2000**, *113* (22), 9901–9904.
- (41) Nosé, S. A Unified Formulation of the Constant Temperature Molecular Dynamics Methods. *J. Chem. Phys.* **1984**, *81* (1), 511–519.
- (42) Jensen, M. B.; Pettersson, L. G. M.; Swang, O.; Olsbye, U. CO₂ Sorption on MgO and CaO Surfaces: A Comparative Quantum Chemical Cluster Study. *J. Phys. Chem. B* **2005**, *109* (35), 16774–16781.
- (43) Dung, N. T.; Unluer, C. Performance of Reactive MgO Concrete under Increased CO₂ Dissolution. *Cem. Concr. Res.* **2019**, *118*, 92–101.
- (44) Unluer, C. Carbon Dioxide Sequestration in Magnesium-Based Binders. *Woodhead Publishing*. **2018**, 129–173.
- (45) Mutisya, S. M.; Kalinichev, A. G. Carbonation Reaction Mechanisms of Portlandite Predicted from Enhanced Ab Initio Molecular Dynamics Simulations. *Minerals* **2021**, *11* (5), 509.